8. Langeveld CH, van Waas MP, Stoof JC, et al. Implication of glucocorticoid receptors in the stimulation of human glioma cell proliferation by dexamethasone. *J Neurosci Res* 1992;31:524–531.
9. Gibelli N, Zibera C, Butti G, et al. Hormonal modulation of brain tumor growth: a cell culture study. *Acta Neurochir (Wien)* 1989;101:129–133.
10. Guerin C, Wolff JE, Laterra J, Drewes LR, Brem H, Goldstein GW. Vascular differentiation and glucose transporter in rat gliomas: effects of steroids. *Ann Neurol* 1992;31:481–487.
11. Di Chiro G. Positron emission tomography using [^{18}F] fluoro-deoxyglucose in brain tumors: a powerful diagnostic and prognostic tool. *Invest Radiol* 1986;22:360–371.
12. Hölzer T, Herholz K, Jeske J, Heiss WD. FDG-PET as a prognostic indicator in radiochemotherapy of glioblastoma. *J Comput Assist Tomogr* 1993;17:681–687.
13. Francavilla TL, Miletich RS, Di Chiro G, Patronas NJ, Rizzoli HV, Wright DC. Positron emission tomography in the detection of malignant degeneration of low-grade gliomas. *Neurosurgery* 1989;24:1–5.
14. Ishizu K, Nishizawa S, Yonekura Y, et al. Effects of hyperglycemia on FDG uptake in human brain and glioma. *J Nucl Med* 1994;35:1104–1109.
15. Ralston ML, Jennrich RI. Dud, a derivative-free algorithm for non-linear least squares. *Technometrics* 1978;20:7–14.
16. Patlak CS, Blasberg RG, Fenstermacher JD. Graphical evaluation of blood-to-brain transfer constants from multiple-time uptake data. *J Cereb Blood Flow Metabol* 1983;3:1–7.
17. Lucignani G, Schmidt KC, Moresco RM, et al. Measurement of regional cerebral glucose utilization with fluorine-18-FDG and PET in heterogeneous tissues: theoretical considerations and practical procedure. *J Nucl Med* 1993;34:360–369.
18. Phelps ME, Huang SC, Hoffman EJ, et al. Tomographic measurement of local cerebral glucose metabolic rate in humans with [^{18}F]2-fluoro-2-deoxy-d-glucose: validation of method. *Ann Neurol* 1979;6:371–388.
19. Spence AM, Graham MM, Muzi M, et al. Deoxyglucose lumped constant estimated in a transplanted rat astrocytic glioma by the hexose utilization index. *J Cereb Blood Flow Metab* 1990;10:190–198.
20. DeLaPaz RL, Patronas NJ, Brooks RA, et al. PET study of suppression of gray-matter glucose-utilization by brain tumors. *AJNR* 1983;4:826–829.
21. Herholz K, Rudolf J, Heiss WD. FDG transport and phosphorylation in human gliomas measured with dynamic PET. *J Neurooncol* 1992;12:159–165.
22. Fulham MJ, Brunetti A, Aloj L, Raman R, Dwyer AJ, Di Chiro G. Decreased cerebral glucose metabolism in patients with brain tumors: an effect of corticosteroids. *J Neurosurg* 1995;83:657–664.
23. Leenders KL, Beaney RP, Brooks DJ, Lammertsma AA, Heather JD, McKenzie CG. Dexamethasone treatment of brain tumor patients: effects on regional cerebral blood flow, blood volume, and oxygen utilization. *Neurology* 1985;35:1610–1616.
24. Axelrod L. Inhibition of prostacyclin production mediates permissive effect of glucocorticoids on vascular tone. *Lancet* 1983;i:903–906.
25. Luthert PJ, Greenwood. Experimental studies and the blood-brain barrier. In: Capildeo R, ed. *Steroids in diseases of the central nervous system.* New York: Wiley & Sons; 1989;47–57.
26. Nagakawa H, Groothuis DR, Owens ES, Fenstermacher JD, Patlak CS, Blasberg RG. Dexamethasone effect on [^{125}I] albumin distribution in experimental RG-2 gliomas and adjacent brain. *J Cereb Blood Flow Metabol* 1987;7:687–701.
27. Hawkins RA, Mans AM, Davis DW, Hibbard LS, Lu DM. Glucose availability to individual cerebral structures is correlated to glucose metabolism. *J Neurochem* 1983;40:1013–1018.
28. Heiss WD, Pawlik G, Herholz K, et al. Regional kinetic constants and cerebral metabolic rate for glucose in normal human volunteers determined by dynamic positron emission tomography of [^{18}F]2-fluoro-2-deoxy-D-glucose. *J Cereb Blood Flow Metabol* 1984;4:212–223.
29. Herholz K, Ziffling P, Staffen W, et al. Uncoupling of hexose transport and phosphorylation in human gliomas demonstrated by PET. *Eur J Cancer Clin Oncol* 1988;24:1139–1150.
30. Oldendorf WH. Expression of tissue isotope distribution. *J Nucl Med* 1974;15:725–726.

Organ-Specific Insulin Resistance in Patients with Noninsulin-Dependent Diabetes Mellitus and Hypertension

Ikuo Yokoyama, Tohru Ohtake, Shin-ichi Momomura, Katsunori Yonekura, Nobuhiro Yamada, Junichi Nishikawa, Yasuhito Sasaki and Masao Omata

The Second Department of Internal Medicine, the Department of Radiology, and the Third Department of Internal Medicine, University of Tokyo, Tokyo, Japan.

Abnormal heart and skeletal muscle glucose metabolism in diabetes or essential hypertension has been demonstrated. However, the role of hypertension in heart and skeletal muscle glucose utilization in diabetes has not been clarified yet. **Methods:** We compared heart and skeletal muscle glucose utilization using PET and the whole-body glucose disposal rate (GDR) during insulin clamping in 9 patients with noninsulin-dependent diabetes mellitus (NIDDM) and essential hypertension and 11 patients with NIDDM without hypertension to examine the effect of hypertension on heart and skeletal muscle glucose utilization. Results also were compared with those for 8 asymptomatic healthy control participants. **Results:** Skeletal muscle glucose utilization rate was comparable between hypertensive NIDDM patients (61.2 ± 55.5 $\mu mol \cdot min^{-1} \cdot kg^{-1}$) and normotensive NIDDM patients (50.9 ± 25.2 $\mu mol \cdot min^{-1} \cdot kg^{-1}$) but was significantly reduced in both groups compared with control subjects (94.2 ± 57.3 $\mu mol \cdot min^{-1} \cdot kg^{-1}$), as was the GDR (25.2 ± 11.3 and 24.0 ± 7.5 $\mu mol \cdot min^{-1} \cdot kg^{-1}$), respectively, for patients compared with 38.5 ± 11.5 $\mu mol \cdot min^{-1} \cdot kg^{-1}$ for control participants). However, the myocardial glucose utilization (MGU) rate was significantly reduced in NIDDM patients without hypertension (389 ± 185 $\mu mol \cdot min^{-1} \cdot kg^{-1}$) than in those with hypertension (616 ± 86.4 $\mu mol \cdot min^{-1} \cdot kg^{-1}$, $p < 0.01$). Multivariate stepwise regression analysis has shown that MGU was significantly correlated with systolic blood pressure and plasma free fatty acid concentration. **Conclusion:** Whole-body insulin resistance was observed in NIDDM patients independent of hypertension. The MGU rate may have different properties to oppose insulin resistance than glucose utilization of skeletal muscle in hypertensive patients with NIDDM.

Key Words: glucose metabolism; insulin resistance; diabetes mellitus; hypertension; PET; fluorodeoxyglucose

J Nucl Med 1998; 39:884–889

A recent investigation has revealed that reactivity to insulin between heart and skeletal muscle varies among several diseases, some of which usually are thought to be associated with insulin resistance (*1*). Furthermore, it has been suggested that glucose utilization may vary between heart and skeletal muscle according to the specific disorder (*1–3*). For example, there is increased myocardial glucose utilization (MGU) but reduced skeletal muscle glucose utilization (SMGU) in patients with mild hypertension (*1*). Reduced glucose utilization in the heart but preserved skeletal muscle (*2*) also have been reported. These observations strongly suggest that the kinetics of cardiac muscle glucose utilization may be different from that of SMGU in patients with insulin resistance.

Received Mar. 11, 1997; revision accepted Aug. 5, 1997.
For correspondence or reprints contact: Ikuo Yokoyama, MD, 7-3-1 Hongoh Bunkyo-ku, Tokyo 113, Japan.

Because insulin-activated glucose transporters are distributed primarily in adipose tissue and skeletal muscle (*4,5*), glucose handling in both skeletal muscle and adipose tissue might be essential to developing insulin resistance. Although both insulin-independent and insulin-dependent glucose transporters are present in approximately equal amounts on cardiac myocytes (*6*), the details of the regulation of myocardial glucose handling remain uncertain.

Insulin resistance plays a central role among the many factors contributing to the pathogenesis of noninsulin-dependent diabetes mellitus (NIDDM) and to the development of atherosclerosis in patients with essential hypertension. Because hypertension is often associated with diabetes mellitus, it may be inferred that when these two diseases coexist, insulin resistance would be more severe than if only diabetes or hypertension were present. However, the effect of hypertension on cardiac muscle glucose utilization and SMGU in patients with NIDDM is not clear.

PET has been used extensively in research on the quantitative analysis of glucose metabolism in the brain (*7*), heart (*8*) and skeletal muscle (*1,2*) using fluorine-18-fluorodeoxyglucose (^{18}FDG) as the tracer. By taking advantage of the fact that PET allows simultaneous collection of data for tissue glucose utilization in the heart and skeletal muscle, we succeeded in quantifying differences in cardiac muscle glucose utilization and SMGU between patients with NIDDM who did and did not have hypertension to address the specific role of high blood pressure on cardiac muscle glucose utilization and SMGU.

MATERIALS AND METHODS

Patients and Control Subjects

We studied 20 patients with NIDDM (15 men, 5 women; mean age 54.9 ± 10.9 yr) and eight asymptomatic age-matched healthy control subjects (6 men, 2 women; mean age 53.2 ± 8.1 yr). Of the 20 patients, 9 had essential hypertension. All patients with hypertension were controlled with antihypertensive agents, which included calcium antagonists, angiotensin-converting enzyme inhibitors or both. The 20 patients with NIDDM were treated only with diet therapy. All medication was stopped 8 hr before the study. General characteristics of study participants are shown in Tables 1 and 2. A significant difference was found only in hemoglobin A1c fasting plasma glucose concentration between the control participants and the diabetic patients. Systolic blood pressure was significantly higher in hypertensive diabetic patients than in normotensive diabetic patients. Before the study, we informed all study participants of the nature of the study, after which they agreed to participate in the study protocol, which was approved by the local ethics committee.

Insulin Clamping and Estimation of Whole-Body Insulin Resistance

Quantitative estimation of whole-body insulin resistance was made by obtaining the glucose disposal rate (GDR; in μmol · min^{-1} · kg^{-1}) during insulin clamping 2–3 hr after the beginning of insulin infusion. Insulin clamping was done by simultaneous infusion of regular insulin at a fixed rate (1 mU · kg^{-1} · min^{-1}) and 20% glucose at a variable rate to maintain plasma concentration of glucose at an equilibrium of approximately 100 mg/dl. The infusion rate of 20% glucose was changed every 5 min during the insulin clamping until the GDR achieved a steady state. Because it usually takes 2–3 hr after the initiation of insulin clamping for the GDR to become constant, we used the average GDR 2–3 hr after the initiation of insulin clamping as an indicator of whole-body insulin resistance.

PET

Cardiac muscle glucose utilization and SGMU rates were measured using PET (Headtome IV, Shimadzu Corp., Kyoto, Japan) and ^{18}F-FDG. The Headtome IV has seven imaging planes. The in-plane resolution is 4.5 mm at FWHM, and the z-axial resolution is 9.5 mm at FWHM. The effective in-plane resolution is 7 mm after using a smoothing filter. The sensitivities of the Headtome IV scanner are 14 and 24 kHz (μCi/ml) for direct and cross-planes, respectively.

Acquisition of Myocardial Metabolic Images

After waiting 120 min to allow for the blood glucose concentration to remain constant, we injected ^{18}F-FDG (185–370 MBq) and collected dynamic data for 1 hr 45 sec. During this interval, we obtained 19 dynamic scans using the following protocol: five 15-, three 30-, four 120-, four 300- and three 600-sec scans.

Quantification of Tissue Glucose Utilization Rate

The amount of glucose metabolized by various organs was determined by calculating the tissue glucose utilization rate. Following the method previously reported by Ohtake et al. (*9*), we obtained the input function from the time–activity curve of the descending aorta corrected by seven venous blood samplings. Using the input function, we determined $k_1 * k_3/(k_2 + k_3)$ with Patlack graphic analysis and calculated the tissue glucose utilization rate by substituting $k_1 * k_3/(k_2 + k_3)$ in the following equation:

$$\text{Tissue glucose utilization rate} = [k_1 * k_3/(k_2 + k_3)] * (\text{Blood glucose concentration})/3/\text{lumped constant.} \quad \text{Eq. 1}$$

The values k_1, k_2, k_3 and k_4 were rate constants of the following chemical formula:

$$\text{Glucose(serum)} \underset{k_2}{\overset{k_1}{\rightleftarrows}} \text{Glucose(myocardium)} \underset{k_4}{\overset{k_3}{\rightleftarrows}} \text{Glucose-6-phosphate,} \quad \text{Eq. 2}$$

where k_4 is assumed to be zero in the myocardium and skeletal muscle.

The blood glucose concentration was measured from the arterialized vein three times during the dynamic scan using ^{18}F-FDG. The average of these values was used for calculating the tissue glucose utilization rate. The lumped constant was calculated to be 0.67 in cardiac myocytes (*10*), as reported for animal experiments. The lumped constant in skeletal muscle cells was assumed to be 1.0, as used in previous studies using PET and ^{18}F-FDG (*1,2*).

All data were corrected for dead-time effects to reduce errors to less than 1%. To avoid the influence of the partial volume effect associated with the objects' size, we used recovery coefficients obtained from experimental phantom studies in our laboratory. The recovery coefficient was 0.8 when myocardial wall thickness was 10 mm. To correct for partial volume effect, wall thickness was measured with two-dimensional echocardiography by specialists in our hospital. The recovery coefficients were taken into consideration in our program to measure the tissue glucose utilization rate.

We obtained the MGU rate from the transaxial images. The MGU for each participant was determined by averaging the values of seven slices. We also obtained the SMGU rate from the back muscle using the transaxial dynamic data of seven slices. The total amount of SMGU was determined by averaging these values.

To calculate the tissue glucose utilization rate, we used the Taitan high-speed image processing system (Asahi Kasei Information System Co., Ltd., Tokyo, Japan) and Dr. View software (Asahi Kasei Information System Co., Ltd.). PET data were collected under insulin clamping as described earlier.

TABLE 1
Participant Characteristics

Variable	Control	Noninsulin-dependent diabetes mellitus	p
No. of patients (male/female)	8 (6/2)	20 (15/5)	—
Age (yr)	53.2 ± 8.1	54.9 ± 10.9	ns
Body weight (kg)	63.6 ± 4.9	63.0 ± 9.77	ns
Height (cm)	161.0 ± 7.2	163 ± 8.24	ns
Body mass index	24.3 ± 2.5	23.9 ± 2.78	ns
Systolic BP (mmHg)	122.0 ± 8.6	135.0 ± 19.4	ns
Diastolic BP (mmHg)	72.0 ± 6.5	77.0 ± 11.5	ns
RPP	9013 ± 1756	9101 ± 1899	ns
Insulin (μU/ml)	69.1 ± 29.2	63.0 ± 24.6	ns
Free fatty acid concentration (mEq/liter)	0.32 ± 0.19	1.12 ± 0.85	<.05
Hemoglobin A1c (%) (mol/liter)	5.7 ± 0.30	8.26 ± 1.65	<0.01
Fasting plasma blood glucose concentration (mol/liter)	4.87 ± 0.48	8.75 ± 2.49	<0.01
Total cholesterol (mol/liter)	5.14 ± 0.67	4.88 ± 0.64	ns
HDL cholesterol (mol/liter)	1.41 ± 0.79	1.09 ± 0.23	ns
Triglycerides (mol/liter)	1.28 ± 0.41	2.06 ± 1.83	ns
LDL cholesterol (mol/liter)	3.18 ± 0.55	2.78 ± 0.96	ns

ns = not significant; RPP = rate pressure products.

TABLE 2
Characteristics of NIDDM Patients With and Without Hypertension

Variable	Normal blood pressure	Hypertension
No. of patients	11	9
Age (yr)	51.8 ± 12.3	59.2 ± 6.63
Body weight (kg)	64.3 ± 8.7	62.3 ± 11.7
Height (cm)	169 ± 6.2	158 ± 7.2*
Body mass index	23.2 ± 2.20	24.7 ± 3.51
Hemoglobin A1c (%)	8.9 ± 1.8	8.3 ± 1.4
Insulin	57.7 ± 22.3	71.4 ± 15.2
Free fatty acid concentration (mol/liter)	1.12 ± 0.67	1.04 ± 1.15
Fasting plasma-blood glucose concentration (mol/liter)	10.1 ± 2.2	8.9 ± 1.8
Total cholesterol (mol/liter)	4.71 ± 0.62	4.93 ± 0.61
HDL cholesterol (mol/liter)	1.13 ± 0.24	1.06 ± 0.24
Triglycerides (mol/liter)	1.83 ± 1.20	1.61 ± 1.19
LDL cholesterol (mol/liter)	2.69 ± 0.67	2.74 ± 1.20
Systolic BP (mmHg)	126 ± 10.6	150 ± 20.5*
Diastolic BP (mmHg)	73.4 ± 9.2	82.4 ± 8.88*
Heart rate (bpm)	69.5 ± 6.6	60.1 ± 6.6
RPP	8480 ± 1554	9490 ± 1694

Statistical Analysis

Data with two parameters were analyzed with the two-tailed Student's t-test. Data with three parameters were analyzed using an analysis of variance. A probability value of 0.05 was considered statistically significant. Multivariate stepwise regression analysis was used to examine which variables were independently related to MGU among plasma free fatty acid (FFA) concentration, hemoglobin A1c, fasting glucose concentration, total cholesterol, plasma triglycerides, high-density lipoprotein (HDL) cholesterol, low-density lipoprotein (LDL) cholesterol, systolic blood pressure, diastolic blood pressure and age. Values are expressed as mean ± s.d.

RESULTS

Whole-Body Glucose Disposal Rate

The GDR in normotensive diabetics (24.0 ± 7.5 $\mu mol \cdot min^{-1} \cdot kg^{-1}$) was comparable to that in diabetics with hypertension (25.2 ± 11.3 $\mu mol \cdot min^{-1} \cdot kg^{-1}$). The GDR in both groups was significantly reduced compared with controls (38.5 ± 11.5 $\mu mol \cdot min^{-1} \cdot kg^{-1}$, $p < 0.01$).

Skeletal Muscle Glucose Utilization

The SMGU rate in normotensive diabetics (50.9 ± 25.2 $\mu mol \cdot min^{-1} \cdot kg^{-1}$) also was comparable to that in hypertensive diabetics (61.2 ± 55.5 $\mu mol \cdot min^{-1} \cdot kg^{-1}$), but in both groups it was significantly lower than in control subjects (94.2 ± 57.3 $\mu mol \cdot min^{-1} \cdot kg^{-1}$, $p < 0.01$).

Myocardial Glucose Utilization

The MGU rate in the normotensive group (389 ± 185 $\mu mol \cdot min^{-1} \cdot kg^{-1}$) was significantly reduced compared with that in both hypertensive diabetic subjects (600 ± 122 $\mu mol \cdot min^{-1} \cdot kg^{-1}$, $p < 0.01$) and control subjects (614.6 ± 161.5 $\mu mol \cdot min^{-1} \cdot kg^{-1}$; Table 3). The MGU rate was correlated with systolic ($r = 0.50$, $p < 0.05$; Fig. 1) and diastolic ($r = 0.60$, $p < 0.01$; Fig. 2) blood pressure. However, there was no significant relationship between the MGU rate and the rate pressure products.

Serum Glucose Concentration

During insulin clamping, the average serum glucose concentration in diabetics (4.90 ± 0.73 mmol/liter) was the same as that of control participants (4.87 ± 0.48 mmol/liter).

Serum Insulin Concentration

Serum insulin concentration after insulin clamping in NIDDM patients (63.0 ± 24.6 μU/ml) was comparable to that in control participants (69.1 ± 29.2 μU/ml). There was no significant difference between the serum insulin concentration at the beginning and end of dynamic PET scanning.

Serum Free Fatty Acid Concentration

The serum FFA concentration during the insulin clamping in NIDDM patients (1.12 ± 0.85 mEq/liter) was significantly higher than that of control subjects (0.32 ± 0.19 mEq/liter, $p < 0.05$). However, there was no significant difference between normotensive NIDDM patients (1.22 ± 0.73 mEq/liter) and hypertensive NIDDM patients (1.00 ± 1.01 mEq/liter). There was a significant inverse relationship between the MGU rate and plasma FFA concentration in NIDDM patients ($r = -0.58$, $p < 0.05$; Fig. 3). Multivariate stepwise regression analysis showed that systolic blood pressure and plasma FFA concentration were independently related to the MGU rate ($r = 0.742$, $p < 0.01$) among plasma FFA concentration, hemoglobin A1c, fasting glucose concentration, total cholesterol, plasma triglycerides, HDL cholesterol, LDL cholesterol, systolic blood pressure, diastolic blood pressure and age.

TABLE 3
Comparison of Whole-Body Insulin Resistance and Heart and Skeletal MGU Rates Among NIDDM Without Hypertension and NIDDM With Hypertension and Controls

NIDDM (NT) (n = 11)	NIDDM (HT) (n = 9)	Control (n = 8)
GDR 24.0 ± 7.5*	25.2 ± 11.3*	38.5 ± 11.5
SMGU 42.7 ± 21.1*	51.3 ± 46.6*	94.2 ± 57.3
MGU 389 ± 185*†	600 ± 122	614.6 ± 161.5

*$p < 0.05$ compared with control.
†$p < 0.01$ compared with NIDDM (HT).
GDR = glucose disposal rate ($\mu mol \cdot min^{-1} \cdot kg^{-1}$); SMGU = skeletal muscle glucose utilization ($\mu mol \cdot min^{-1} \cdot kg^{-1}$); MGU = myocardial glucose utilization ($\mu mol \cdot min^{-1} \cdot kg^{-1}$); NIDDM = noninsulin-dependent diabetes mellitus; NT = normotensive; HT = hypertensive.

DISCUSSION

Results of this study show that: (a) whole-body insulin resistance occurred independently of hypertension in patients with NIDDM; (b) both the MGU and SMGU rates were reduced in normotensive NIDDM patients; and (c) the MGU rate was significantly reduced in NIDDM patients without hypertension compared with both controls and NIDDM patients with hypertension.

Skeletal Muscle Glucose Utilization in Patients with NIDDM

Several investigators have found that whole-body insulin resistance is strongly related to impaired SMGU rates (*11,12*). Therefore, reduced SMGU rates in patients with NIDDM are consistent with these findings. Because of the association between insulin resistance and hypertension, it is important to investigate the influence of hypertension on insulin resistance in patients with NIDDM. However, we found that both whole-body insulin resistance and SMGU rates were not altered by hypertension in patients with NIDDM. Therefore, the mechanism that provokes insulin resistance in patients with NIDDM may differ from that of hypertension.

Myocardial Glucose Utilization in Patients with NIDDM

Insulin resistance in the myocardium was present but was less severe than whole-body and skeletal muscle insulin resistance in normotensive patients with NIDDM. On the other hand, MGU rates in hypertensive patients with NIDDM were preserved, indicating that myocardial insulin resistance was not present in NIDDM patients with hypertension. This result is consistent with a recent report of increased MGU rates but reduced SMGU rates in patients with nondiabetic mild hypertension (*1*). These findings suggest that there is an important mechanism by which glucose is incorporated into the myocardium that differs from that in skeletal muscle. Certainly, skeletal muscle may play a central role in insulin resistance (*11,12*), whereas the myocardium may have some alternative mechanism to oppose insulin resistance that may partially contribute to a salvage effect to decrease glucose concentration in diabetics. Recently, increased expression of glucose transporter Type 1 in the heart but not in the skeletal muscle in nondiabetic hyperinsulinemic glucose transporter Type 4 (GLUT4)-null mice was reported (*2*). Those supporting systems in the myocardium may contribute to increased MGU rates in the event of ischemia or in patients with hypertension. Preserved insulin-responsive glucose transporter gene expression in skeletal muscle also has been reported (*13*). The results suggest that insulin resistance in NIDDM patients may not only be attributable to a GLUT4 deficit in skeletal muscle cells but also to impaired cellular signal transduction systems between the insulin receptor and Golgi apparatus. Those reports may relate to our results.

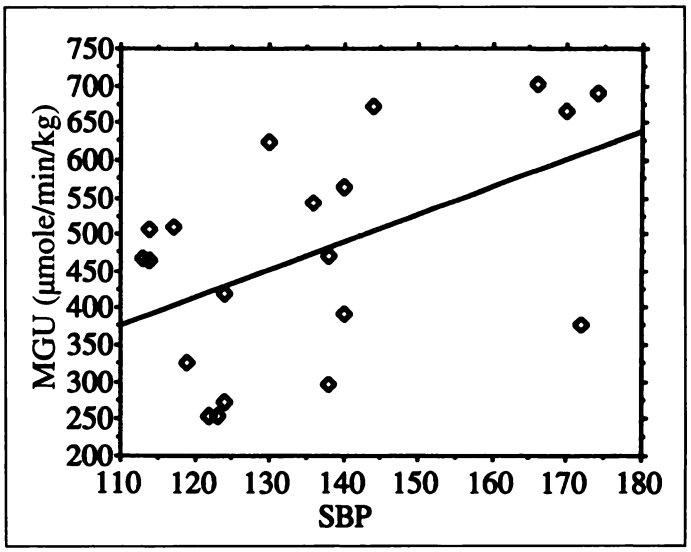

FIGURE 1. Significant relationship between MGU rate and systolic blood pressure.

Relationship with Plasma Free Fatty Acid Concentration

It has been suggested that the MGU rate is inversely correlated with the plasma FFA level. In this study, a significant inverse relationship between these two parameters was found. However, the plasma FFA level was comparable between hypertensive and normotensive patients with NIDDM, so the increased plasma FFA concentration in NIDDM patients cannot be the cause of the difference in MGU rates between the two. Plasma FFA may influence MGU rates in normotensive patients with NIDDM only through the so-called Randle's cycle (*14*). On the other hand, there might be an unknown mechanism to uptake glucose in the myocardium to oppose increased FFA concentration in patients with hypertensive NIDDM.

Relationship Between Myocardial Glucose Utilization Rates and Blood Pressure

There was a significant relationship between MGU rates and both systolic and diastolic pressure. However, there was no significant relationship between rate pressure products and MGU rates in patients with NIDDM. These data suggest that

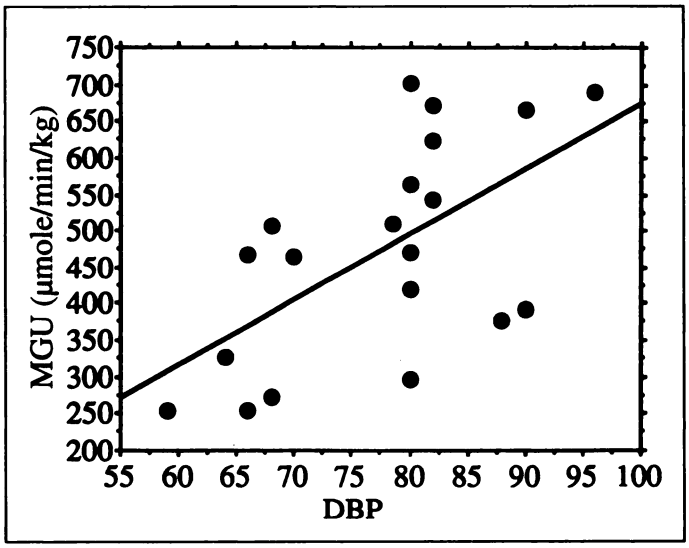

FIGURE 2. Significant relationship between MGU rate and diastolic blood pressure.

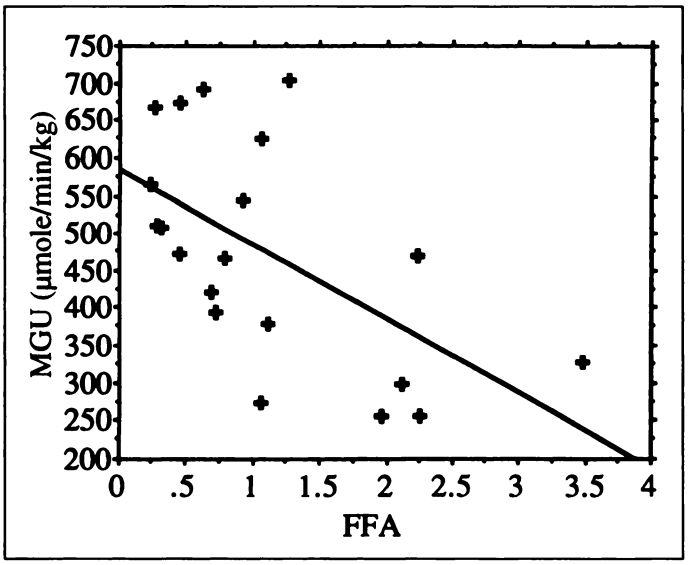

FIGURE 3. Significant relationship between MGU rate and plasma FFA concentration.

preserved MGU rates in hypertensive NIDDM patients may not simply be explained by the increase in myocardial oxygen demand. Actually, hypertension might increase oxygen demand, which could increase MGU rates, as reported by Nuutila et al. (*1*). The cause for this discrepancy is speculative. Our hypertensive NIDDM patients may have had a more severe hypertensive status than the patients with mild hypertension used by Nuutila et al. (*1*), and the diabetic status might have altered the myocardial cellular glucose handling in response to hypertension. It also is possible that the durations of the hypertensive state and the antihypertensive therapy would alter MGU rates. For instance, a relatively longer hypertensive state and shorter antihypertensive therapy would increase MGU rates much more than a shorter hypertensive state and longer antihypertensive therapy. Those matters might alter the relationship between RPP and MGU rates in patients with NIDDM. Furthermore, the plasma FFA concentration in both of the NIDDM groups was increased more than twofold compared with that of control subjects, so the myocardium might use FFA as the predominant source of energy for oxidative metabolism. Myocardial oxidative metabolism should be explained mainly by FFA metabolism, and the contribution of MGU rates on oxidative metabolism may become relatively small when the FFA level is high. That may preclude a correlation between MGU rates and oxygen demands.

Measurement of Tissue Glucose Metabolism Using PET and Fluorine-18-FDG

To determine SMGU rates, we used a value of 1.0 as the lumped constant according to the report by Pulkki et al. (*2*). When the SMGU rate is calculated relative to GDR assuming that skeletal muscle accounts for 35% of total body weight and that the SMGU rate corresponds to approximately 75% of GDR, the SMGU rate can be estimated as follows: normotensive diabetic subjects, 51 ± 16; hypertensive diabetic subjects, 54 ± 25; and control subjects, 97 ± 29. Those results were similar to the PET results. Therefore, accuracy of the method to determine SMGU rates with PET and ^{18}F-FDG is assured. To determine MGU rates, we used a value of 0.67 as the lumped constant because several studies on MGU rates in diabetes used this value (*2,15*). Although several similar studies of heart and skeletal muscle glucose utilization used this value (*1, 9, 16–21*), it has not been clear whether the lumped constant differs between controls and patients with NIDDM. That is one limitation of this type of study. Further investigation should be done on this point.

Correction of the recovery coefficient was made according to two-dimensional echocardiography. Because overestimation due to left ventricular hypertrophy in hypertensive NIDDM patients should be negligible when the recovery coefficient is estimated, correction of MGU rates by the left ventricular mass index should not be needed.

Insulin Clamping and Myocardial FDG PET

Although the myocardium uses FFA as a primary source of energy under fasting, it uses glucose as a primary source of energy after intake of glucose through induction of endogenous insulin (*16*). Although oral glucose loading is useful for myocardial ^{18}F-FDG imaging, it is difficult to apply to diabetics (*15*). Insulin clamping can maintain serum glucose concentrations constant at the level of fasting, the effects of glucose intolerance are avoided and there is improved imaging accuracy (*17*). In addition, because insulin clamping also allows a steady state, it offers the advantage of eliminating problems concerning quantitative analysis. Several problems associated with myocardial ^{18}F-FDG imaging can be overcome when insulin clamping is used and careful examination of disease status is considered. Our results might contribute to the improvement of diagnostic accuracy of quantitative myocardial ^{18}F-FDG studies.

CONCLUSION

Whole-body insulin resistance in NIDDM patients occurred independently of hypertension. However, heart muscle glucose handling was different between diabetic subjects with hypertension and those without. Alternative mechanisms to oppose myocardial insulin resistance were suggested in NIDDM and hypertension. This approach, using PET and insulin clamping, might be helpful to further the understanding of pathophysiological and biochemical features in patients with NIDDM.

ACKNOWLEDGMENT

This work was supported by the Research Grant for Cardiovascular Disease (8A-5) from the Ministry of Health and Welfare.

REFERENCES

1. Nuutila P, Maeki M, Laine H, et al. Insulin action on heart and skeletal muscle glucose uptake in essential hypertension. *J Clin Invest* 1995;96:1003–1009.
2. Voipio-Pulkki LM, Nuutila P, Kunuuti J. Heart and skeletal muscle glucose disposal in Type 2 diabetic patients as determined by positron emission tomography. *J Nucl Med* 1993;34:2064–2067.
3. Katz EB, Stenbit AE, Hatton K, DePinho R, Charron MJ. Cardiac and adipose tissue abnormalities but not diabetes in mice deficient in GLUT4. *Nature* 1995;337:151–155.
4. Piper RC, Hess LJ, and James DE. Differential sorting of two glucose transporters expressed in insulin-sensitive cells. *Am J Physiol* 1991;260:C570–C580.
5. Goodyear LJ, Hirshman MF, Smith RJ, Horton ES. Glucose transporter number, activity, and isoform content in plasma membranes of red and white skeletal muscle. *Am J Physiol* 1991;260:E556–E561.
6. Rodnick KJ, Henriksen EJ, James DE, Holloszy JO. Exercise training, glucose transporters, and glucose transport in rat skeletal muscles. *Am J Physiol* 1992;262: C9–C14.
7. Patlack CS, Blasberg RG, Fenstermacher JD. Graphical evaluation of blood to brain transfer contents from multiple time uptake data. *J Cereb Blood Flow Metab* 1983;3:1–7.
8. Phelps ME, Hoffman EJ, Selin CE, et al. Investigation of (F-18)2-fluoro-2-deoxyglucose for the measurement of myocardial glucose metabolism. *J Nucl Med* 1978;19: 1311–1319.
9. Ohtake T, Kosaka N, Watanabe T, et al. Noninvasive method to obtain input function for measuring tissue glucose utilization of thoracic and abdominal organs. *J Nucl Med* 1991;32:1432–1438.
10. Raitib O, Phelps ME, Huang SC, Henze E, Selin CE, Schelbelt HR. Positron tomography with deoxyglucose for estimating local myocardial glucose metabolism. *J Nucl Med* 1982;23:577–586.
11. Defronzo RA, Gunnarsson R, Bjorkman O, Olson M, Wahren J. Effect of insulin on

peripheral and splanchnic glucose metabolism in non-insulin dependent (type II) diabetes mellitus. *J Clin Invest* 1985;76:149–155.
12. Hickey MS, Carey JO, Azevedo JL, et al. Skeletal muscle fiber composition is related to adiposity and in vitro glucose transport rate in humans. *Am J Physiol* 1995;268: E453–E457.
13. Eriksson J, Koranyi L, Bourey R, et al. Insulin resistance in type 2 (non-insulin-dependent) diabetic patients and their relatives is not associated with a defect in Type 2 (non-insulin-dependent) diabetic patients and their relatives is not associated with a defect in the expression of the insulin-responsive glucose transporter (GLUT 4) gene in human skeletal muscle. *Diabetologia* 1992;35:143–147.
14. Randle PJ, Garland PB, Hales CN, Newshholme EA. The glucose fatty acid cycle its role in insulin sensitivity and the metabolic disturbances of diabetes mellitus. *Lancet* April 1963;785–789.
15. Ohtake T, Yokoyama I, Watanabe T, et al. Myocardial glucose metabolism in noninsulin dependent diabetes mellitus patients evaluated by FDG-PET. *J Nucl Med* 1995;36:456–463.
16. Nuutila P, Koivisto VA, Knuuti J, et al. The glucose free fatty acid cycle operates in human heart and skeletal muscle in vivo. *J Clin Invest* 1992;89:1767–1744.
17. Knuuti J, Nuutila P, Ruotsalainen U, et al. Euglycemic hyperinsulinemic clamp and oral glucose load in stimulating myocardial glucose utilization during positron emission tomography. *J Nucl Med* 1992;33:1255–1262.

Three-Dimensional Surface Display of Dynamic Pulmonary Xenon-133 SPECT in Patients with Obstructive Lung Disease

Kazuyoshi Suga, Norihiko Kume, Kazuya Nishigauchi, Yasuhiko Kawakami, Takeo Kawamura, Tsuneo Matsumoto and Naofumi Matsunaga

Department of Radiology, Yamaguchi University School of Medicine, Ube, Yamaguchi, Japan

To better perceive abnormal regional ventilation in patients with obstructive lung disease, a three-dimensional display was applied to dynamic pulmonary ^{133}Xe SPECT. **Methods:** Dynamic SPECT was performed using a triple-detector SPECT system in 30 patients with obstructive disease, 13 patients with restrictive disease and 7 normal subjects. After reconstructing color-illuminated, surface-rendered three-dimensional images of equilibrium and 3-min washout (WO_3), a single three-dimensional fusion display was created from these two different time-course image sets in which a three-dimensional WO_3 image indicating ^{133}Xe retention was transparently visible through three-dimensional equilibrium image delineating lung contours. The three-dimensional equilibrium and WO_3 images were created by a 25% threshold of the ^{133}Xe maximal pixel activity (MPA) in equilibrium data. Besides, a three-dimensional WO_3 image with a 18% threshold [mean + 2 s.d. ratios (%) of the MPA in WO_3 data to that in equilibrium data in normal subjects] was used for assessing the presence of retention compared to normal lungs. **Results:** The 18% threshold three-dimensional WO_3 image showed abnormal retention in obstructive diseases but not in restrictive diseases. The three-dimensional fusion display provided an overview of localized retention in obstructive diseases and enhanced the perception of their spatial relationships and extent compared to those on multislice tomograms. The extent of retention correlated well with $\%FEV_1$ ($r = 0.813$) and ^{133}Xe clearance-time ($T_{1/2}$) ($r = 0.912$). **Conclusion:** This topographic modality for ^{133}Xe SPECT is helpful for the better perception of anatomic distributions of ^{133}Xe retention and inter-study comparisons of ventilation abnormality in patients with obstructive disease.

Key Words: SPECT; xenon-133 gas; lung ventilation; three-dimensional imaging; surface-rendered imaging

J Nucl Med 1998; 39:889–893

Pulmonary dynamic SPECT of ^{133}Xe gas is an effective tool to assess regional ventilation abnormality without superimposition of lung tissues in patients with obstructive lung diseases (*1,2*). However, review and interpretation of multislice tomographic data are often difficult especially for elimination of ^{133}Xe activity in the lungs in washout (WO) phase. If SPECT information was displayed in a realistic three-dimensional form image, it would simplify and improve the interpretation. Several three-dimensional imaging techniques are now available for display of almost all parts of the body (*3–12*). In this study, we challenged a three-dimensional display for ^{133}Xe SPECT, and validated its feasibility in assessing regional ventilation abnormality in obstructive lung diseases.

MATERIALS AND METHODS

Patient Population

The subjects were 30 patients (9 women, 21 men; age range 47–76 yr) with obstructive lung disease including 20 with pulmonary emphysema, 6 with chronic bronchitis and 4 with bronchial asthma. The diagnosis of 20 patients with pulmonary emphysema was based on chest thin-slice, high-resolution CT scan, physical findings and a history of long-term cigarette smoking and pulmonary function tests. Six patients with chronic bronchitis showed focal bronchiectasis on chest CT. Four patients with bronchial asthma were diagnosed by intermittent wheezing and improved pulmonary function tests after administration of a bronchodilator. The mean predicted vital capacity (%VC) and forced expiratory volume in 1 sec ($\%FEV_1$) were 76.2 ± 19.2% and 42.2 ± 9.8%, respectively. Xenon-133 SPECT was repeated after treatment in seven patients including three with pulmonary emphysema treated by thoracoscopic lung volume reduction surgery (*13*) and two each with bronchial asthma and chronic bronchitis treated by a bronchodilator with or without antibiotics.

For comparison, 7 normal subjects (7 men; age range 25–40 yr) with normal pulmonary function tests and chest CT and 13 patients (5 women, 8 men, age range 42–63 yr) with usual interstitial pneumonia were studied. These patients with restrictive disease were histologically diagnosed, and the mean %VC and $\%FEV_1$ were 51.2 ± 7.2% and 79.2 ± 5.4%, respectively. Informed consent was obtained from all the participants.

Dynamic Xenon-133 SPECT and Three-Dimensional Surface Displays

Dynamic SPECT was performed using a continuous repetitive rotating acquisition mode with a triple-detector SPECT system (GCA 9300 A/HG, Toshiba Medical, Tokyo, Japan), as described

Received Dec. 23, 1996; revision accepted Aug. 6, 1997.

For correspondence or reprints contact: Kazuyoshi Suga, MD, Department Radiology, Yamaguchi University School of Medicine, 1144 Kogushi, Ube, Yamaguchi, 755 Japan.